ChemComm



COMMUNICATION

View Article Online
View Journal | View Issue



Cite this: *Chem. Commun.,* 2016, **52**, 5003

Received 30th December 2015, Accepted 3rd March 2016

DOI: 10.1039/c5cc10643e

www.rsc.org/chemcomm

X-ray absorption study of ceria nanorods promoting the disproportionation of hydrogen peroxide†

Tai-Sing Wu,‡^{ab} Yunyun Zhou,‡^c Renat F. Sabirianov,^d Wai-Ning Mei,^d Yun-Liang Soo*^{ab} and Chin Li Cheung*^c

A quasi *in situ* X-ray absorption study demonstrated that the disproportionation of hydrogen peroxide (H_2O_2) promoted by ceria nanorods was associated with a reversible Ce^{3+}/Ce^{4+} reaction and structural transformations in ceria. The direction of this reversible reaction was postulated to depend on the H_2O_2 concentration and the fraction of Ce^{3+} species in ceria nanorods.

Fluorite-structured cerium oxide (or ceria) nanomaterials have attracted great interest from chemistry, materials and engineering communities because of their broad applications in catalysis, 1-3 sensors, 4 biomedicine, 5 and fuel cells. 6 Ceria has long been known to generate reactive oxygen species by catalyzing the disproportionation of hydrogen peroxide (H_2O_2). This system has displayed enhanced catalytic activities towards the degradation of pollutants. 7,8 Ceria nanomaterials have also been reported to scavenge free oxygen radicals and reduce toxic H_2O_2 molecules in biological systems. 9 These chemical properties of ceria nanomaterials have been ascribed to the interconversion of the cerium ions between their +3 and +4 states coupled with the formation of oxygen vacancy defects in ceria. 10,11 However, this proposed reaction mechanism is still under intense debates. 7-9,12

The ability to monitor the chemical state transformation of cerium in ceria during reactions is critical to understand the structure–activity relationships of ceria nanomaterials. Currently, the determination of chemical state transformation of cerium in ceria in aqueous reactions is still challenging, largely because of the interference of water molecules in the measurements. X-ray photoelectron spectroscopy (XPS) and UV-Vis spectroscopy have

In situ X-ray absorption spectroscopy (XAS) has been regarded as a versatile tool to elucidate changes in atomic structures and oxidation states of catalysts during reactions. ¹⁴ For example, Wang *et al.* utilized this technique to illustrate metallic copper in the Cu/ceria catalyst as the active species in catalyzing the water gas shift reaction. ¹⁵ Quasi *in situ* XAS techniques have also been applied in catalysis studies to overcome challenges such as chemical compatibility of reactors and strong photon absorption by reactors in the implementations of *in situ* XAS techniques. ^{14,16} For instance, Bergmann *et al.* applied the quasi *in situ* XAS technique to reveal reversible structural changes of a crystalline Co₃O₄ catalyst in an oxygen evolution reaction. ¹⁶

Herein we report our quasi in situ XAS study of the oxidation states of cerium and the local structures in ceria nanorods upon catalyzing the disproportionation of H₂O₂. Ceria nanorods were selected over ceria nanoparticles in this study because they are often reported to have higher catalytic activities. 1,17 In our XAS experiments, a wet chemical environment enabled by a tris(hydroxymethyl)aminomethane (Tris) buffer solution was employed to prevent the reaction system from drying out and to maintain the pH of the system. Since the reaction mechanism strongly depends upon the pH of the reaction, 7,18 this method allows reliable quantitative evaluation of reaction species in ceria samples. 11,19,20 Our study revealed reversible changes in the oxidation states of cerium and local atomic structures of ceria in the H₂O₂ disproportionation reaction. In our experiments, ceria nanorods were first added to a solution containing 10 mM H_2O_2 and 0.1 M Tris buffer (pH = 7.54) to yield a reaction mixture with a nanorod concentration of 500 mg L^{-1} . Samples of this suspended mixture were pipetted out at various reaction times (T = 10 min to 10 h) to wet filtered papers which were then analyzed by XAS. A control experiment without H2O2 was used

been applied to evaluate changes in the oxidation states of cerium in ceria after its reaction with aqueous H_2O_2 . However, due to the altered experimental environments such as the vacuum requirement in XPS and limited quantitative capability of UV/Vis spectroscopy, artefacts and misinterpretations in studies using these techniques are often hard to identify.

^a Department of Physics, National Tsing-Hua University, Hsinchu, 30013, Taiwan. E-mail: soo@phys.nthu.edu.tw

^b National Synchrotron Radiation Research Center, Hsinchu, 30013, Taiwan

^c Department of Chemistry, University of Nebraska-Lincoln, Lincoln, NE, 68588, USA. E-mail: ccheung2@unl.edu

^d Department of Physics, University of Nebraska-Omaha, Omaha, NE, 68182, USA

[†] Electronic supplementary information (ESI) available: Experimental details, microstructure and electronic property analysis by TEM, XRD, XPS and XAS. See DOI: 10.1039/c5cc10643e

[‡] These authors contributed equally.

for comparisons. These control data were regarded as our data at T = 0 h (see experimental details in the ESI†).

Communication

The initial morphology, microstructure and chemical state of as-synthesized ceria nanorods^{1,3} were characterized by transmission electron microscopy, X-ray diffraction (XRD) and XPS (see Fig. S1, ESI \dagger). The ceria nanorods were 50–200 nm in length and 5–12 nm in diameter. The XRD pattern of the nanorods was indexed according to the ICDD card 04-013-4361 and was found to display a cubic $Fm\bar{3}m$ structure of CeO₂. The oxidation states of surface cerium atoms were qualitatively analyzed by XPS. The fraction of Ce³⁺ on the surface was determined to be *ca.* 20%, indicating a defective surface structure of this as-synthesized ceria sample (Fig. S3, ESI \dagger).

X-ray absorption near edge structure (XANES) experiments were performed to investigate the redox behavior of ceria nanorods catalyzing the H₂O₂ disproportionation reaction. The Ce L₃-edge XANES spectra of ceria nanorods were collected at different reaction times during a 10 h reaction. Four of the XANES data scanned at the reaction times of 0 h, 0.5 h, 2 h and 10 h are illustrated in Fig. 1. The differences in the intensities of these spectra were demonstrated by the zoomed-in areas of the peaks. The intensity of the XANES spectrum of ceria nanorods significantly decreased in the first 0.5 h. After another 1.5 h of reaction, the intensity returned to its original magnitude. This was indicated by the XANES data collected at T = 2 h, which had a similar intensity to the one at T = 0 h. As the reaction further proceeded, the XANES spectrum at T = 10 h demonstrated negligible changes in both the spectral intensity and shape when compared with those at T = 0 h and T = 2 h.

To reveal the changes in the Ce oxidation state, a quantitative analysis was performed by curve-fitting the XANES spectra with an arctangent function to simulate the edge jump and Gaussian functions for peak features^{21–23} (Fig. 2a). The center of the arctangent function was set at the inflection point of the main edge. Peaks A and B at 5737.7 eV and 5730.8 eV were associated with the Ce^{4+} ions in ceria, corresponding to the $2p4f^05d^*$ and

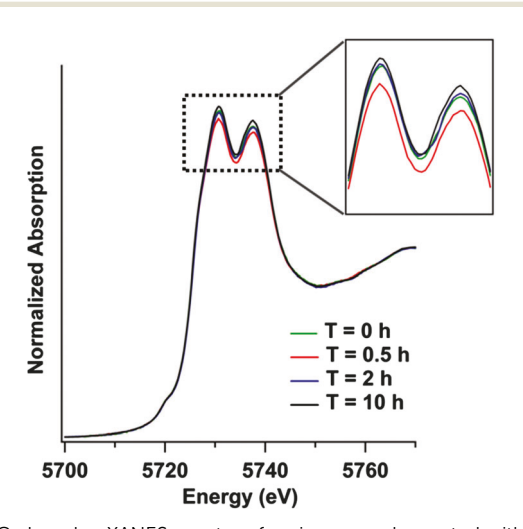


Fig. 1 Ce L_3 -edge XANES spectra of ceria nanorods reacted with 10 mM H_2O_2 at different reaction times: \mathcal{T} = 0 h, 0.5 h, 2 h and 10 h. (inset) Zoomed-in peak areas.

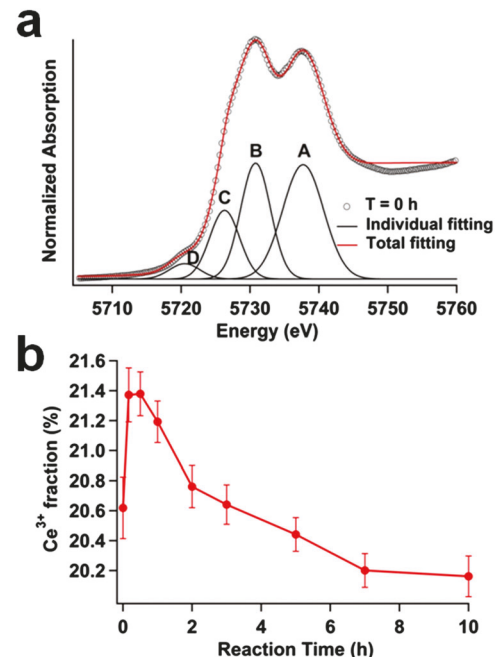


Fig. 2 Quantitative analysis of quasi *in situ* characterization of ceria nanorods. (a) Ce L_3 -edge XANES spectrum and fitting peaks of ceria nanorods in 0.1 M Tris buffer solution without H_2O_2 . Peaks A and B were ascribed to the Ce^{4+} state. Peak C was due to the Ce^{3+} state. Peak D was assigned to the final states of $2p4f^*$. (b) Ce^{3+} fraction in ceria nanorods as a function of reaction time in the $10 \text{ mM } H_2O_2/0.1 \text{ M}$ Tris buffer solution.

2p4f¹5d*L final states, respectively. While 2p denotes the hole produced in 2p³/2, 5d* refers to the presence of an excited electron in the 5d band, and L represents a ligand hole in the anion orbital. Peak C, at 5726.3 eV, was associated with the Ce³+ valence state. Peak D, located at 5720.5 eV in the pre-edge region, was assigned to the final states of 2p4f*, which was forbidden by the selection rule due to a 5d ad-mixture with the 4f state. With a delocalized d character at the bottom of the conduction band due to the cubic crystal-field splitting of Ce 4f states, the transition was partially allowed to appear as a small peak. 4f* referred to the presence of an excited electron in the 4f band.

The Ce L₃-edge XANES spectra of all samples showed the coexistence of Ce³⁺ and Ce⁴⁺ states, with the Ce⁴⁺ state being dominant in all samples. The fractions of Ce³⁺ and Ce⁴⁺ in the samples were calculated using the following equations:

$$[Ce^{3+}] = A(Ce^{3+})/(A(Ce^{3+}) + A(Ce^{4+}))$$

$$[Ce^{4+}] = A(Ce^{4+})/(A(Ce^{3+}) + A(Ce^{4+}))$$

where $A(Ce^{3+})$ and $A(Ce^{4+})$ were the total integrated peak areas corresponding to the Ce^{3+} and Ce^{4+} XANES signals, respectively. According to Fig. 2b, the Ce^{3+} fraction (expressed in percentage) in ceria nanorods increased from 20.6% at T=0 h to 21.4% at T=0.5 h. It then slowly decreased to 20.8% at T=2 h. After a 3 h-reaction, the Ce^{3+} fraction approached 20.6%, which was very similar to its original value. During the reaction period between 3 h and 10 h, the overall percentage of Ce^{3+} kept

ChemComm

decreasing but varied insignificantly. It stayed at around the level of 20.2% at the end of reaction. Note that the changes in the Ce³⁺ fraction detected by XANES were not likely due to the adsorption of Ce ions from the dissolution of ceria onto ceria nanorods. Our inductively coupled plasma-mass spectrometry studies concluded that the concentration of Ce ions in the

reaction mixtures was less than 1 ppb (see details in the ESI†).

In summary, during the 10 h long H_2O_2 disproportionation reaction, the surface Ce^{4+} of ceria nanorods was reduced to Ce^{3+} by the H_2O_2 molecules in the beginning of the first 0.5 h, and then was slowly oxidized back to Ce^{4+} in the next 9 h. The surface reaction in aqueous solutions was governed by the surface potential and the overall redox potential of ceria and H_2O_2 . High concentration of H_2O_2 exhibited high reduction potential and thus was expected to reduce surface Ce^{4+} to Ce^{3+} at the beginning. The slow oxidative process of ceria was likely due to the oxidizing power of H_2O_2 , which became dominant after a dramatic decrease of H_2O_2 concentration in the solution. In addition, the defective ceria surface with high concentration of Ce^{3+} decreased the reduction potential of the ceria surface, and was postulated to enable ceria to be oxidized by H_2O_2 .

Local structures surrounding Ce atoms were probed using the extended X-ray absorption fine structure (EXAFS) technique. The experimental data were analyzed using the *IFEFFIT* software package. The Fourier transforms of Ce L₃-edge k^3 -weighted $\chi(k)$ of EXAFS spectra depicted the changes in the local structure of Ce atoms with respect to the reaction time (Fig. 3 and Fig. S4, ESI†). The fitting parameters of EXAFS spectra are shown in Table 1 and Table S1 (ESI†). The as-synthesized ceria nanorods exhibited a coordination number of 5.8 in the first Ce–O shell. An extra peak appeared at around 1.65 Å after the addition of hydrogen peroxide. Owing to the "shortness" of this R value, this peak could be attributed to the presence of superficial chemical structures with a Ce—O bond, possibly similar to the one reported in a cerium($_{\rm IV}$) oxo complex, [Ce— $_{\rm OL}$ ($_{\rm DEI}$)₂($_{\rm H_2}$ O)]·MeC(O)NH₂.²⁷

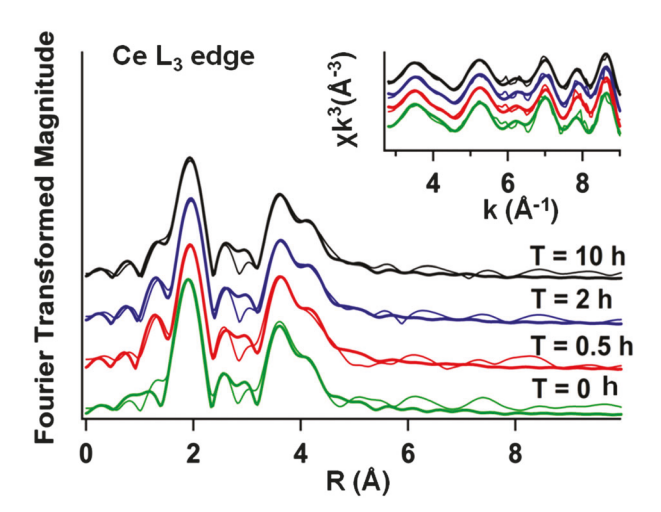


Fig. 3 Fourier transformed Ce L_3 -edge EXAFS data of ceria nanorod sample with different reaction times in 10 mM $H_2O_2/0.1$ M Tris buffer solution. The inset shows the corresponding EXAFS spectra in k-space. Data: thick lines; fittings: thin lines.

This peak attained its highest intensity at T=0.5 h. The intensity then slowly decreased after 2 h reaction time until T=10 h. This trend was consistent with the changes in Ce^{3+} fraction from XANES data analysis, indicating the modification of local structures caused by reactions with H_2O_2 . The coordination number of the Ce–O bond at 2.34 Å reached its minimum value of 4.7 at T=0.5 and 2 h, and slowly increased to 5.8 at T=10 h, which was closer to that of ceria samples before reaction (*i.e.* at T=0 h).

The redox cycle of the ceria sample revealed by the EXAFS data agreed well with the intensity changes in the XANES data, implying a reduction-and-oxidation cycle of ceria with $\rm H_2O_2$ during the 10 h reaction. Based on our XANES and EXAFS results, we proposed that ceria underwent a redox cycle process in the Fenton-like reaction with $\rm H_2O_2$ as follows:

Ceria reduction process:

$$Ce^{4+} + H_2O_2 \rightarrow Ce^{3+} + HO_2^{\bullet} + H^+$$
 (1)

Ceria oxidation processes:

$$2Ce^{3+} + H_2O_2 + 2H^+ \rightarrow 2Ce^{4+} + 2H_2O$$
 (2)

$$4Ce^{3+} + O_2 + 4H^+ \rightarrow 4Ce^{4+} + 2H_2O$$
 (3)

In a concentrated H_2O_2 solution, H_2O_2 molecules were proposed to serve as reducing agents and convert the surface Ce^{4+} to Ce^{3+} , resulting in the increase of Ce^{3+} fraction and the decrease of an average coordination number of oxygen atoms around Ce atoms at 2.34 Å.

The hydroperoxyl radical (HO_2^{\bullet}) byproduct in eqn (1) was known to involve in the conversion of the Ce oxidation state in ceria. ^{7,28} Besides the reaction species described in eqn (1), other reactive oxygen species such as O_2^{\bullet} , 1O_2 , O_2^- and OH^{\bullet} had been proposed to form in the reduction reaction. ^{7,9,11} These unstable oxygen species could undergo interconversions with each other through electron transfers. Overall, these species altered the surface coordination and chemical potential of ceria, and therefore regulated the chemical states of cerium in ceria

Table 1 Fitted structural parameters of the Ce L_3 -edge EXAFS analysis for ceria nanorod samples reacting with 10 mM $H_2O_2/0.1$ M Tris buffer solution. N is the coordination number around the central atoms. R is the average bond distance. σ^2 is the Debye–Waller factor. Italic marks indicate fixed parameters in the fitting analysis

Ceria nanorods reaction time	Atom	N	R (Å)	$\sigma^2 \left(10^{-3} \text{ Å}^2\right)$
T = 0 h	O Ce	5.8 ± 0.6 5.6 ± 0.4	2.30 ± 0.01 3.83	$4.7 \pm 1.2 \\ 1.8 \pm 0.6$
T = 0.5 h	O O Ce	$\begin{array}{c} 0.9 \pm 0.3 \\ 4.7 \pm 0.4 \\ 4.7 \pm 0.4 \end{array}$	$1.65 \pm 0.02 \ 2.32 \pm 0.01 \ 3.83$	3.9 ± 0.8 3.9 ± 0.8 1.3 ± 0.3
<i>T</i> = 2 h	O O Ce	0.7 ± 0.2 4.7 ± 0.3 4.5 ± 0.3	$1.66 \pm 0.02 \ 2.33 \pm 0.01 \ 3.83$	3.6 ± 0.8 3.6 ± 0.8 0.6 ± 0.4
<i>T</i> = 10 h	O O Ce	0.7 ± 0.3 5.8 ± 0.4 4.9 ± 0.3	1.68 ± 0.03 2.33 ± 0.01 3.83	6.6 ± 0.8 6.6 ± 0.8 1.1 ± 0.4

nanorods during the reaction. A slight reduction of its pH value from 7.54 to 7.41 in this system was observed after the first 10 min of the reaction. This finding supported our hypothesis that Ce^{4+} in ceria were reduced to Ce^{3+} by H_2O_2 and H_3O^+ were produced in this reaction. Our finding corroborated similar observations of pH reduction by Wang *et al.* in their study of

Communication

H₂O₂ disproportionation catalyzed by nanoceria.¹¹ As the reaction proceeded, the concentration of H₂O₂ decreased and ceria nanorods possessed significant population of Ce3+ on their surfaces. These two factors led to changes in solution potential and ceria surface potential, which consequently promoted the oxidation of Ce3+ to Ce4+ by H2O2 molecules (eqn (2)). During the H_2O_2 decomposition process, a lot of bubbles which were ascribed to oxygen evolution were observed. This increased the partial pressure of oxygen which could also oxidize the ceria surface (eqn (3)). Overall, these factors possibly gave rise to the decrease in the Ce³⁺ fraction and an increase in the Ce-O coordination number at 2.3 Å as indicated by our EXAFS data. Furthermore, the coordinatively unsaturated Ce sites, which were indirectly inferred from the increase in Ce³⁺ fraction, might also provide reactive sites for the adsorption of peroxide species and participate in the disproportionation of H₂O₂ molecules.¹¹

Our hypothesized redox cycle could also be conjectured from the reported Pourbaix diagram of the $Ce(III/IV)-H_2O-H_2O_2$ aqueous system. Depending on the pH of solutions, H_2O_2 concentration and the surface potential of ceria, H_2O_2 could exhibit dual behavior, either acting as an oxidizing agent or a reducing agent. Dehavior, either acting as an oxidizing agent or a reducing agent. The standard potentials of H_2O_2/HO_2^{\bullet} and Ce^{4+}/Ce^{3+} are 1.5 V and 1.44 V, respectively. The similarity of these two electrochemical potentials potentially permitted the reversible reaction (eqn (1)–(3)) to occur because the concentration of H_2O_2 and the Ce^{3+} fraction of the nanorod surface changed during the catalyzed reaction.

To summarize, we demonstrated the application of a quasi in situ XAS technique to elucidate the changes in chemical states of cerium and local structures in ceria nanorods in their reaction with $\rm H_2O_2$. Our measurements under wet conditions allowed reliable analysis of chemical states of cerium and the structures in ceria due to minimal environmental modifications and disturbance to the ceria nanorods. The observed reversible structural changes of ceria nanorods were strongly correlated with the $\rm Ce^{3^+}/\rm Ce^{4^+}$ conversion and changes in the $\rm H_2O_2$ concentration.

The authors are grateful for the financial support from the National Science Foundation (CHE-1362916). We acknowledge the National Synchrotron Radiation Research Center, Nebraska Center of Materials and Nanoscience, Cornell Center for Materials Research and Rare Earth Salts for the use of their facilities.

Notes and references

- N. J. Lawrence, J. R. Brewer, L. Wang, T. S. Wu, J. Wells-Kingsbury,
 M. M. Ihrig, G. H. Wang, Y. L. Soo, W. N. Mei and C. L. Cheung,
 Nano Lett., 2011, 11, 2666–2671.
- 2 Y. Zhou, N. J. Lawrence, L. Wang, L. M. Kong, T. S. Wu, J. Liu, Y. Gao, J. R. Brewer, V. K. Lawrence, R. F. Sabirianov, Y. L. Soo, X. C. Zeng, P. A. Dowben, W. N. Mei and C. L. Cheung, *Angew. Chem., Int. Ed.*, 2013, 52, 6936–6939.
- 3 Y. Zhou, N. J. Lawrence, T. S. Wu, J. Liu, P. Kent, Y. L. Soo and C. L. Cheung, *ChemCatChem*, 2014, 6, 2937–2946.
- 4 N. Izu, S. Nishizaki, W. Shin, T. Itoh, M. Nishibori and I. Matsubara, Sensors, 2009, 9, 8884–8895.
- 5 C. Xu and X. G. Qu, NPG Asia Mater., 2014, 6, e90.
- 6 S. D. Park, J. M. Vohs and R. J. Gorte, Nature, 2000, 404, 265-267.
- 7 P. F. Ji, L. Z. Wang, F. Chen and J. L. Zhang, ChemCatChem, 2010, 2, 1552–1554.
- 8 Y. C. Wang, X. X. Shen and F. Chen, J. Mol. Catal. A: Chem., 2014, 381, 38–45.
- S. M. Hirst, A. S. Karakoti, R. D. Tyler, N. Sriranganathan, S. Seal and C. M. Reilly, *Small*, 2009, 5, 2848–2856.
- 10 C. Walkey, S. Das, S. Seal, J. Erlichman, K. Heckman, L. Ghibelli, E. Traversa, J. F. McGinnis and W. T. Self, *Environ. Sci.: Nano*, 2015, 2, 33–53.
- 11 Y. J. Wang, H. Dong, G. M. Lyu, H. Y. Zhang, J. Ke, L. Q. Kang, J. L. Teng, L. D. Sun, R. Si, J. Zhang, Y. J. Liu, Y. W. Zhang, Y. H. Huang and C. H. Yan, *Nanoscale*, 2015, 7, 13981–13990.
- 12 J. M. Perez, A. Asati, S. Nath and C. Kaittanis, Small, 2008, 4, 552-556.
- 13 M. Das, S. Patil, N. Bhargava, J. F. Kang, L. M. Riedel, S. Seal and J. J. Hickman, *Biomaterials*, 2007, 28, 1918–1925.
- 14 A. I. Frenkel, J. A. Rodriguez and J. G. G. Chen, ACS Catal., 2012, 2, 2269–2280.
- 15 X. Wang, J. A. Rodriguez, J. C. Hanson, D. Gamarra, A. Martínez-Arias and M. Fernández-García, J. Phys. Chem. B, 2006, 110, 428–434.
- 16 A. Bergmann, E. Martinez-Moreno, D. Teschner, P. Chernev, M. Gliech, J. F. de Araujo, T. Reier, H. Dau and P. Strasser, *Nat. Commun.*, 2015, 6, 8625.
- 17 X. Du, D. Zhang, L. Shi, R. Gao and J. Zhang, J. Phys. Chem. C, 2012, 116, 10009–10016.
- 18 P. Salgado, V. Melin, D. Contreras, Y. Moreno and H. D. Mansilla, J. Chil. Chem. Soc., 2013, 58, 2096–2101.
- 19 A. M. Shahin, F. Grandjean, G. J. Long and T. P. Schuman, *Chem. Mater.*, 2005, 17, 315–321.
- 20 F. Zhang, P. Wang, J. Koberstein, S. Khalid and S. W. Chan, Surf. Sci., 2004, 563, 74–82.
- 21 R. C. Karnatak, J. M. Esteva and H. Dexpert, *Phys. Rev. B: Condens. Matter Mater. Phys.*, 1987, 36, 1745–1749.
- 22 H. Dexpert, R. C. Karnatak, J. M. Esteva, J. P. Connerade, M. Gasgnier, P. E. Caro and L. Albert, Phys. Rev. B: Condens. Matter Mater. Phys., 1987, 36, 1750-1753.
- 23 A. Bianconi, A. Marcelli, H. Dexpert, R. Karnatak, A. Kotani, T. Jo and J. Petiau, Phys. Rev. B: Condens. Matter Mater. Phys., 1987, 35, 806–812.
- 24 F. F. Munoz, L. M. Acuna, C. A. Albornoz, A. G. Leyva, R. T. Baker and R. O. Fuentes, *Nanoscale*, 2015, 7, 271–281.
- 25 G. Kaindl, G. Schmiester, E. V. Sampathkumaran and P. Wachter, Phys. Rev. B: Condens. Matter Mater. Phys., 1988, 38, 10174-10177.
- 26 M. Newville, J. Synchrotron Radiat., 2001, 8, 322-324.
- 27 Y. M. So, G. C. Wang, Y. Li, H. H. Y. Sung, I. D. Williams, Z. Y. Lin and W. H. Leung, *Angew. Chem., Int. Ed.*, 2014, 53, 1626–1629.
- 28 P. B. Sigler and B. J. Masters, *J. Am. Chem. Soc.*, 1957, **79**, 6353–6357.
- 29 P. Yu, S. A. Hayes, T. J. O'Keefe, M. J. O'Keefe and J. O. Stoffer, J. Electrochem. Soc., 2006, 153, C74–C79.